J Therm Anal Calorim (2014) 118:1331–1338
DOI 10.1007/s10973-014-4226-0

Study of thermo-oxidative chemical pre-treatment of isotactic polypropylene

Rasa Alaburdaitė · Valentina Krylova

Received: 14 February 2014 / Accepted: 21 September 2014 / Published online: 16 October 2014

Abstract A thermo-oxidative pre-treatment with chemical solutions is required in order to provide the adherence of inorganic semiconductor to the isotactic polypropylene (iPP) surface. A few thin films of iPP were treated with oxidizing solution at 90 °C. The crystalline properties were analyzed using XRD, and it had shown the presence of the α-monoclinic phases. The ATR-FTIR spectra had indicated that characteristic iPP peaks after thermo-oxidative chemical pre-treatment diminished sharply. Moreover, the new carbonyl groups (C = O) were observed, which signified oxidation. The UV–Vis spectra had showed a blue shift in the absorption edge, which corresponded to decrease in the optical band gap. The non-isothermal decomposition and crystallization kinetics of iPP films were studied and compared by means of thermogravimetric analysis and differential scanning calorimetric measurement. The values of the melting temperature T_m and the crystallization temperature T_c were found to be iPP surface structure and heating/cooling rate dependent. The activation energy of crystallization E_c was determined.

Keywords Isotactic polypropylene film · Thermo-oxidative chemical treatment · ATR-FTIR · Non-isothermal crystallization kinetics · Activation energy

Introduction

Polymers modified by thin electrically conductive or semiconductive films of binary inorganic compounds, particularly of metal chalcogenides [1–4], represent a new class of materials—composites. Composite materials possess tunable characteristic optical and semiconducting properties. In the recent years, metal chalcogenide semiconducting thin films on polymeric surfaces have been extensively studied due to their technological applications [3, 4].

PP is one of the fastest growing classes of thermoplastics and can serve as a model of the metal chalcogenide–polymer composite. PP among other polymers possesses some exceptional properties. It has the highest stiffness, the highest melting point, and the best physical characteristics (lightness, mechanical strength, and electro- and thermal insulating capabilities) [5–7]. PP is resistant toward many organic and inorganic solvents and chemicals. However, in its intrinsic state, PP does not possess the surface properties required for preparation of thin film composites [8]. In one unit of PP molecule chain, three atoms of carbon exist in the form of different groups such as $–CH_2–$, >CH–, and $–CH_3$. This results in the three-dimensional structure of the molecule existing in a variety of forms which differ in their spatial arrangement. Isotactic, syndiotactic, and atactic forms are the three corresponding structures for polypropylene [9–11]. iPP is known to have three semicrystalline modifications such as α-monoclinic, β-hexagonal, and γ-orthorhombic forms. In a usage iPP films as the substrates for depositing semiconducting films, a serious drawback of PP material is its hydrophobicity and low free surface energy [12]. It results in a weak molecular interaction between the composite components. The free energy of PP material surface can be increased by creating new oxygen-containing functional chemical groups such as –OH and –COOH on the material surface layer [8, 12–15]. This task has been fulfilled by employing different approaches such as chemical, electrochemical, physical, and plasma methods [16–18]. Although these methods of polymer surface

R. Alaburdaitė (✉) · V. Krylova
Department of Physical and Inorganic Chemistry, Kaunas University of Technology, Radvilenų str. 19, 50254 Kaunas, Lithuania
e-mail: Rasa.Alaburdaite@ktu.lt

modification are different and quite complicated, in general all surface modification techniques share the common goal of controlling the nature and number of chemical functional groups on the polymer surface.

One of the PP surface modification methods is its oxidation. The oxidation of iPP in solid phase can be achieved via reactions with ozone, γ-initiated corona method and UV ray or with chemical oxidizing mixture [12, 16, 19–23]. The oxidation of iPP leads to the formation of oxygen-containing surface functional groups, which greatly affect the surface polarity and the adhesion properties of the polymer toward the metal chalcogenide deposition.

The chemical oxidation method can be easily conducted as it does not require specialized equipment and hence can be easily adopted in any small-scale laboratory.

Generally, chemical etching involves the usage of the mixtures of chromic acid and potassium permanganate in sulfuric acid to introduce reactive oxygen-containing moieties into PP and bring about improvement in adhesion. Additionally, oxidizers convert smooth hydrophobic polymer surfaces to rough hydrophilic surfaces by dissolving the amorphous regions and/or oxidizing the surface. It has been established that the amorphous phase on the interfacial layers is the one mainly affected during these treatments. As it has been reported earlier, high etching time leads to over-etched sample where the surface strength is diminished and peel strength dropped [24]. Thus, the investigation of the iPP surface in terms of functional group content, crystallinity, and activation energy of the etched surface is significant for systematic understanding of metal chalcogenides formation on PP surface.

The aim of this work was to determine the physico-chemical characteristics of thermo-oxidative chemically treated commercial PP. The compositional, structural, and optical properties were determined by means of the ATR-FTIR, UV–Vis, XRD, TG, and DSC techniques. The obtained results are important knowledge for the optimization of metal chalcogenide–PP composite deposition conditions.

Experimental

Materials and sample preparation

15 × 70 mm size samples of commercial PP film (Proline X998, KWH Plast, Finland) of 150 μm thickness were used for the experiments. Density of the PP samples was determined by float method in water–acetone solutions of various densities (0.900–0.950 g cm^{-3}) at 20 °C. It has been established that the density of the initial PP is $\rho = 0.905$ g cm^{-3}.

For depositing metal chalcogenide layer, the hydrophobic PP sample requires an initial surface treatment process in order to facilitate its hydrophilicity. PP mass losses after chemical treatment are recommended to be 2 g m^{-2} [25, 26]. With aspiration to avoid over-etching, it was recommended [25] to prepare etching solution with phosphoric acid (H_3PO_4). It has been determined that in order to obtain the recommended weight losses, oxidizing solution (H_2SO_4/H_3PO_4 (1:1), saturated with CrO_3) at 90 °C temperature and 25 min treatment is suitable. After thermo-oxidative chemical pre-treatment, the density of PP changed to $\rho = 0.910$ g cm^{-3}, indicating that amorphous PP with lower density and molecular mass was etched and washed from PP surface.

All solutions were prepared using distilled water and analytical grade reagents H_2SO_4 (96 %, Barta a Cihlar, Czech Republic), H_3PO_4, (60 %, Lach-Ner, Czech Republic), and CrO_3 (>99 %, Reachim, Russia). Only freshly prepared solutions were used for measurements and were not de-aerated during the experiments. Thus, obtained samples were removed from the reaction solution, rinsed with distilled water, and dried at room temperature.

Test methods

X-ray diffraction (XRD)

The XRD patterns of PP film samples were recorded with a conventional Bragg–Brentano geometry (θ–2θ scans) on a DRON-6 automated diffractometer equipped with a secondary graphite monochromator. Cu Kα radiation ($\lambda = 1.541838$ Å) was used as a primary beam. The patterns were recorded from 10 to 60° 2θ in steps of 0.02° 2θ, with the measuring time of 0.5 s per step. The diffraction patterns were recorded automatically by a data acquisition system. The peaks obtained were identified on the basis of those available in PDF-2 data base [27].

UV–Vis spectroscopy

The UV–Vis spectra (195–600 nm) were recorded using a Spectronic Genesys 8 UV/Visible spectrophotometer.

FTIR spectroscopy

The changes in chemical structure and binding configuration were analyzed by attenuated total reflectance (ATR) spectroscopy, since ATR spectroscopy is an often chosen technique as it may be used to obtain the spectra of the surfaces of the adhesive sides of a sample. ATR-FTIR spectra were recorded in the wavenumber range of 3,000–600 cm^{-1} on a Perkin Elmer FTIR Spectrum GX

spectrophotometer by averaging 64 scans with a wave number resolution of 1 cm^{-1} at room temperature.

Thermogravimetric analysis (TG)

The non-isothermal TG measurements were carried out using 6–7 mg of the polymer samples at a heating rate of 10 °C min^{-1} in nitrogen atmosphere using a Netzsch instrument "STA 409 PC Luxx." The flow rate of nitrogen atmosphere was: purge gas—100 cm^3 min^{-1}, protective gas—30 cm^3 min^{-1}. Each sample was scanned over a temperature range from 30 °C up to 500 °C. The mass change was recorded as a function of temperature. Ceramic sample holders and Al crucibles were used.

Differential scanning calorimetry (DSC)

The DSC tests of PP film samples were performed using a Perkin Elmer DSC 8500 (with Hyper DSC). Polymers with a thickness of 150 μm were punched-cut with a standard single-hole paper puncher. Disk-like samples of about 4 mg were weighed and sealed into Perkin Elmer aluminum DSC pans. All tests were performed in a nitrogen atmosphere. The flow rate of nitrogen atmosphere was 50 cm^3 min^{-1}. All samples were first heated to 250 °C at different rates (5, 10, 15, and 20 °C min^{-1}) and kept for 3 min to eliminate prior thermal history. The specimen was subsequently cooled down to 30 °C at the same cooling rate.

Results and discussion

PP identification by X-ray diffraction analysis

The surface structure of initial PP film used in experiments was identified by XRD analysis. Figure 1 presents the X-ray diffraction pattern in conventional mode (θ–2θ) of the initial and oxidized PP film samples. The peaks of semicrystalline PP between 10 and 60° (in 2θ) were observed. These peaks, in accordance with JCPDS 50-2397, appear at 14.00°, 16.85°, 18.47°, 21.01°, and 21.80° (in 2θ) that correspond to the (110), (040), (130), (111), and (131) planes, respectively. The X-ray diffraction of initial PP has shown the typical α-form iPP samples [28] and exhibited complete absence of the β-form, which shows two strong peaks at 2θ of 16.28° and 21.28° [29].

After the chemical thermal oxidation of iPP film, diffraction pattern gave dominant peaks at 14.00°, 16.84°, 18.46° (in 2θ), and others as indicated in Table 1. In both initial iPP and oxidized one, the crystal plane of PP is monoclinic, showing reflections assigned to planes (110), (040), and (130) (Table 1).

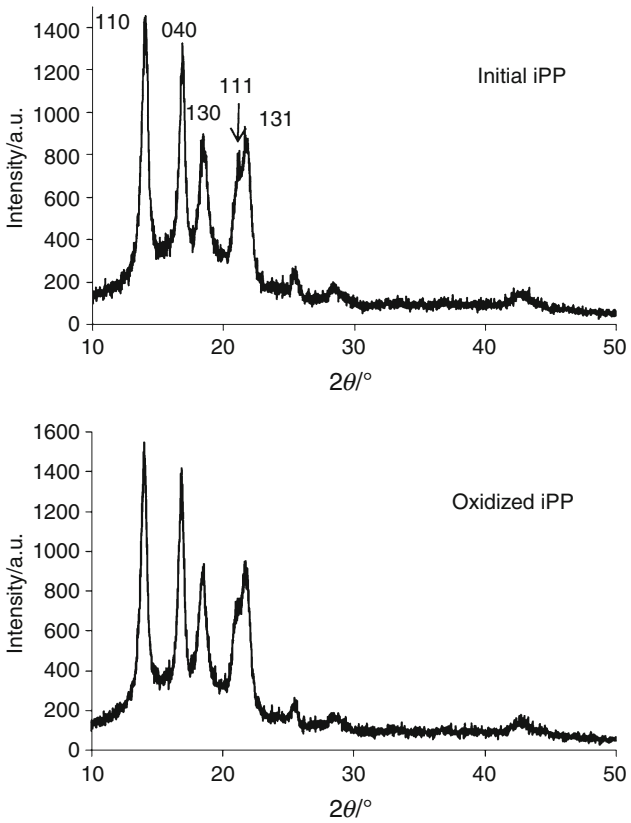

Fig. 1 Comparison of XRD patterns of iPP film

Table 1 The 2θ diffraction angles and (hkl) reflections for the initial and oxidized iPP

Standard 2θ value JCPDS 50-2397 [27]	(hkl)	Observed d-value/Å		Observed 2θ	
		Initial iPP	Oxidized iPP	Initial iPP	Oxidized iPP
14.19	110	6.32	6.32	14.00	14.00
17.05	040	5.26	5.26	16.85	16.84
18.64	130	4.80	4.80	18.47	18.46
21.36	111	4.22	4.23	21.01	20.98
21.87	131/041	4.07	4.07	21.80	21.80
25.70	150/060	3.50	3.49	25.43	25.47
27.25	141/200	3.14	3.15	28.36	28.33

The comparison of XRD spectra indicates that there is no major change observed in the width and positions of XRD peaks after iPP thermal oxidation in chemical solution. The intensity of the (110), (040), (130), (111), and (131) peaks increases with thermal oxidation. The thermal oxidation involves a negligible shift of the iPP peaks to lower 2θ (Table 1). Attenuation length for iPP in the range of 2θ 10–60° [30] varies from 100 to 1000 μm, respectively. The thickness of the investigated PP films is 150 μm, and the information about the crystallinity has

been obtained throughout the whole sample thickness. In the case of this specific oxidative treatment, it is thought that the effect of the short exposure oxidation on the film thickness is negligible; moreover, the obtained data show that the thermal oxidation slightly affects the crystalline structure of iPP. In the longer term, thermal oxidation affects the crystalline structure of PP significantly [31, 32].

UV–Vis spectroscopy measurements

The optical properties of initial iPP and the one after chemical thermo-oxidative pre-treatment were studied by UV–Vis Spectroscopy in the wavelength range of 195–600 nm, e.g., across UV and visible regions. The transmission spectra are shown in Fig. 2. For all iPP samples studied, in the ultraviolet region at 250 nm the transmittance amounts to 85 % for initial iPP and 87 % for oxidized iPP; then it increases in conjunction with the wavelength and may become as high as 95 % at 600 nm in visible region. Transmittance of the oxidized iPP in the visible spectral region is practically the same as that of initial iPP.

According the literature data [33], the wavelength range of the absorption edge for iPP has been found to be within 200–255 nm in the ultraviolet light region. In our case, the absorption edge for the initial iPP was found at a wavelength of about 245 nm. Thermo-oxidative pre-treatment caused the transmittance to shift toward the lower values. An absorption edge is shown in Fig. 2a and was estimated to be 240 nm, thus indicating the existence of a polar group in the polymer matrix. The shift transmittance after thermo-oxidative pre-treatment of iPP is usually associated with chain scission. The blue shift is due to the formation of the carbonyl group (C = O) [34]. This has also been confirmed by the ATR-FTIR spectroscopic analysis. Thus, it can be inferred that thermo-oxidative pre-treatment causes subtle change in the chemical structure of the polymer without resulting in an alteration of its major physical and structural properties.

The blue shift in absorption edges under thermo-oxidative pre-treatment was correlated with the optical band gap E_g according to Tauc's expression [35].

The intersection of the extrapolated spectrum with the abscissa of the plot $(\alpha\eta\nu)^2$ versus $h\nu$ yields the gap wavelength λ_g from which the energy gap was derived. Energy band gaps were found to be 5.3 eV for initial iPP (Fig. 2b) and 5.2 eV for oxidized one (Fig. 2c), which closely agrees with values reported previously [33].

Thus, the optical absorption method was used for providing information about the energy gap [36]. The thickness of initial iPP is 150 μm. The error in the measurement of the thickness of the films is of the order of ±0.1 μm. For determining the wavelength gap, the best linear fit of the

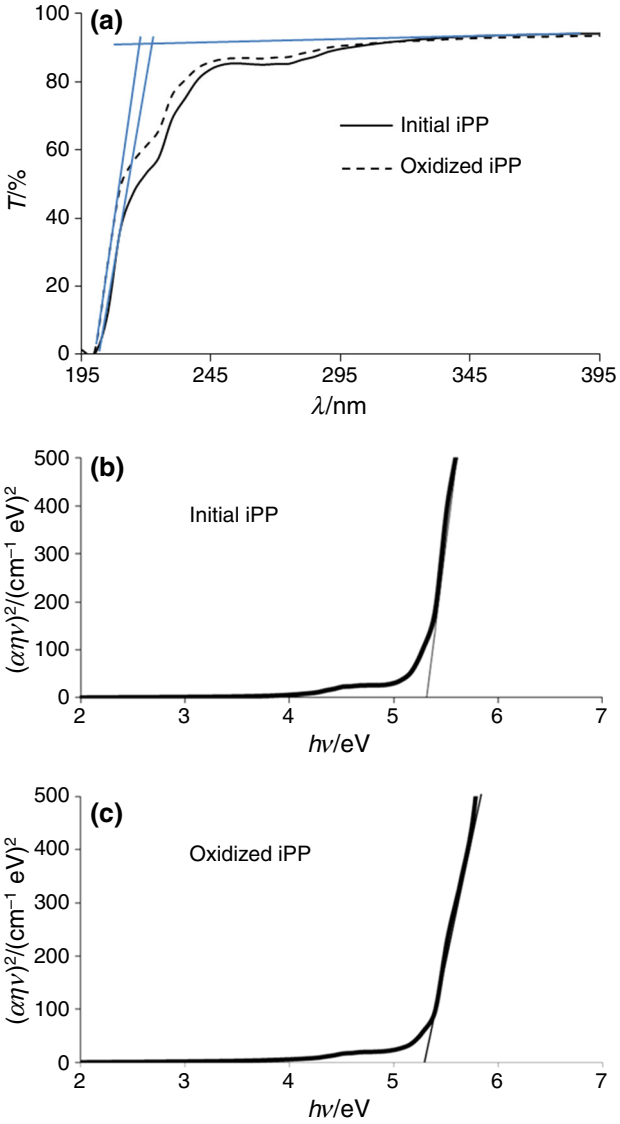

Fig. 2 UV–Vis transmission spectra of initial and oxidized iPP samples (**a**). Direct band gap Tauc plots of initial (**b**) and oxidized (**c**) iPP samples

points on the curve $(\alpha\eta\nu)^2$ versus hν was always performed. Taking into account the accuracy of that fit, the extrapolation toward the band gap wavelength λ_g is possible within an error not exceeding a few %. This corresponds to a maximum possible error in the energy band gap determinations of ±0.1 eV.

Infrared spectroscopy measurements

Figure 3 shows the spectra of initial and oxidized iPP film, obtained with infrared spectrometer (FTIR) in ATR mode. The FTIR analysis enabled identification of the groups' characteristic of iPP used in the experiments. The iPP consists of the repeating propane units (CH_2–$CH(CH_3)$) linked together. The methyl groups (–CH_3) alternate with a

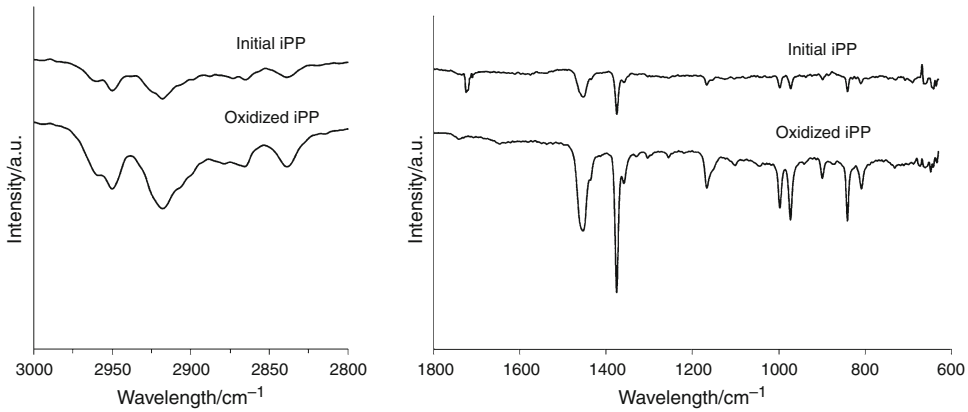

Fig. 3 FTIR spectra (transmittance T vs. wavelength ν) of initial and oxidized iPP samples

hydrogen (H) in the backbone chain and are all on the same side. The FTIR spectrum of the used iPP sample displays absorption peaks which coincide well with the reported literature data [37, 38].

The spectra of initial iPP show the presence of four bands located between 3,000 and 2,800 cm^{-1} (2,948, 2,916, 2,864, and 2,837 cm^{-1}) (Fig. 3a). The peaks corresponding to the methyl group occur at 2,948, 2,864, and 1,375 cm^{-1}. Two peaks at 2,948 and 2,864 cm^{-1} are attributed to the asymmetric stretch vibration and symmetric stretch vibration of C–H. The peaks at 2,916 and 2,837 cm^{-1} are related to methylene group (CH_2) asymmetric and symmetric C–H stretches. In the iPP spectrum, moderate absorption peaks of deformation vibrations of the plane methylene group arise in the spectral range of 1,445–1,485 cm^{-1}, and methyl group vibrations are registered in the range of 1,430–1,470 or 1,365–1,395 cm^{-1}. In the spectrum of iPP under investigation, these peaks appear at 1,451 and 1,375 cm^{-1}, respectively. (Figure 3b). The peak at 1,375 cm^{-1} is due to the known 'umbrella' mode (symmetric bending mode). The peak located at 1,451 cm^{-1} is due to the overlapping of the asymmetric bending mode of the methyl group (CH_3) and the methylene scissoring mode [38].

The absorption peaks at 840, 973, 1,000, and 1,170 cm^{-1} are characteristic vibrations of the terminal-unsaturated CH_2 groups present in iPP [39]. These characteristic features in the spectrum obtained in our experiment are observed at 841, 972, 996, and 1,165 cm^{-1} (Fig. 3b).

The spectrum of oxidized iPP sample shows some changes. The characteristic peaks diminish sharply in intensity and a new signal appears at 1,719 cm^{-1}. This signal is attributed to the carbonyl group (C = O) stretching [36]. The spectrum of oxidized iPP confirms that the chemical thermo-oxidative pre-treatment of iPP increases surface hydrophilicity by introducing oxygen-containing polar groups.

It has reported in literature [40–42] that the volume crystallinity index is proportional to A_{841}/A_{972} ratio, where

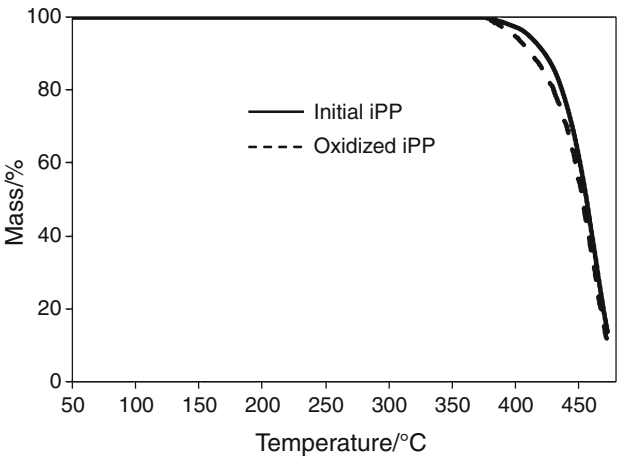

Fig. 4 TG curves of initial and oxidized iPP samples in nitrogen

A_{972} is the absorbance peak intensity at 972 cm^{-1} and is insensitive to the amorphous/crystalline ratio of iPP, whereas A_{841} is the intensity of the band at 841 cm^{-1} linked to crystallinity content. This ratio is close for the initial iPP matrix (0.9966) and oxidized iPP (0.9987) and thus the crystallinity rate is too.

The non-isothermal TG

The TG results obtained from iPP and the oxidized one are shown in Fig. 4. iPP thermally degrades to volatile products above 250 °C through a radical chain process propagated by carbon-centered radicals originated by carbon–carbon bond scission [43]. As seen from Fig. 4, PP volatilizes completely in a single step starting at about 350 °C with a maximum rate at 475 °C. The mass loss of initial PP (87.07 %) takes place very slowly at temperatures below thermal degradation onset (400 °C), but this process occurs very rapidly above 400 °C. The thermal degradation of iPP can take place through random chain scission and a radical chain mechanism.

The process of mass loss of the oxidized iPP (89.87 %) is very similar to mass loss process of initial iPP. Its begins at 350 °C, occurs very rapidly at 375 °C, and is finished at 475 °C.

The non-isothermal DSC

Figure 5 shows the non-isothermal DSC heating/cooling curves of initial iPP. The non-isothermal melting and crystallization parameters of the DSC curves are summarized in Table 2. As shown in Fig. 5, the increase of heating rate from 5 to 20 °C min^{-1}, leads to a decrease in melting peak temperature (T_{mp}) from 162.19 to 160.65 °C. It is well reported that most commercial iPPs are usually blends of different crystal modifications of iPP [44]. Our result could be ascribed to one of α (monoclinic) iPP crystalline forms [45], as has been previously confirmed by XRD and FTIR analyses. In melt-crystallized iPP, crystal structure is the α form too. With the increase of heating rate from 5 to 20 °C min^{-1}, melting enthalpy (ΔH_m) increased. It is evident that the peak of crystallization temperature (T_{cp}) for the initial iPP changed just slightly (from 122.08 to 114.63 °C).

Figure 6 shows the non-isothermal DSC heating/cooling curves of oxidized iPP. T_{mp} and ΔH_m are also listed in Table 2. It can be seen that oxidized iPP shows similar tendency as the initial iPP in T_{mp}, T_{cp}, and ΔH_m.

The crystallinity (X_C) of iPP can be calculated according to the following equations:

$$X_C = \frac{\Delta H_m}{\Delta H_m^0} \cdot 100\,\%, \quad (1)$$

where ΔH_m is the enthalpy of melting of the iPP and ΔH_m^0 is the fusion enthalpy of 100 % crystalline sample (usually the literature value of 209 J g^{-1} is used) [46]. The crystallinity of iPP is calculated from Eq. (1), and the data are listed in Table 3.

It can be seen from Table 3 that thermo-oxidative chemical pre-treatment of iPP does not evidently change the crystallinity. The more severe thermal oxidation influences strongly the iPP crystallinity [31, 32].

The crystallization rate can be expressed as a function of time according to the following equation [47–49]:

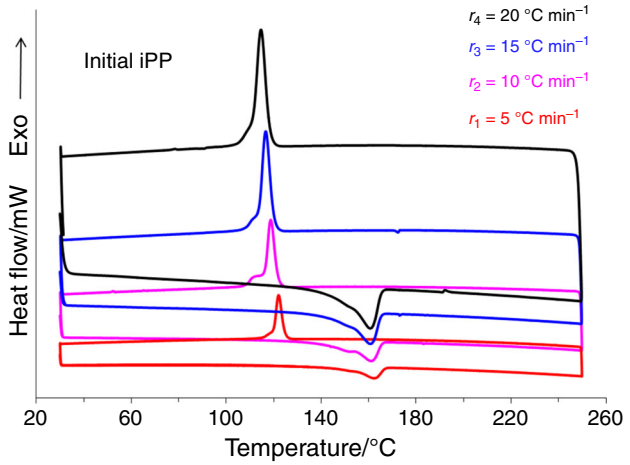

Fig. 5 DSC patterns of initial iPP prepared by non-isothermal melting/crystallization at various heating/cooling rates. The subsequent heating/cooling rates are shown in the figure

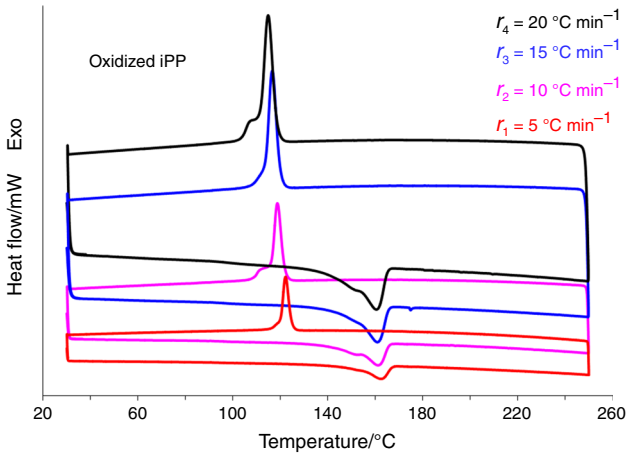

Fig. 6 DSC patterns of oxidized iPP prepared by non-isothermal melting/crystallization at various heating/cooling rates. The subsequent heating/cooling rates are shown in the figure

Table 2 DSC data of iPP

Heating/cooling rate, v_h /°C min^{-1}	T_{mo}/°C*		T_{mp}/°C		ΔH_m/J g^{-1}		T_{cp}/°C		ΔH_c/J g^{-1}	
	Initial iPP	Oxidized iPP	Initial iPP	Oxidized iPP	Initial iPP	Oxidized iPP	Initial iPP	Oxidized iPP	Initial iPP	Oxidized iPP
5	154.71	154.39	162.19	162.20	55.63	61.41	122.08	122.08	−77.17	−84.17
10	142.50	151.26	161.08	161.09	66.17	59.88	118.75	118.65	−80.71	−82.75
15	149.30	153.86	160.69	160.80	66.88	65.68	116.63	116.48	−82.23	−83.73
20	149.91	148.54	160.65	160.37	66.34	63.74	114.63	114.76	−82.27	−82.40

* T_{mo}—Melting onset temperature

Table 3 Non-isothermal crystallization crystallinity of initial and oxidized iPP

Cooling rate, ν_h /°C min^{-1}	Crystallinity, X_C/%	
	Initial iPP	Oxidized iPP
5	26.61	29.38
10	31.66	28.65
15	32.00	31.42
20	31.74	30.49

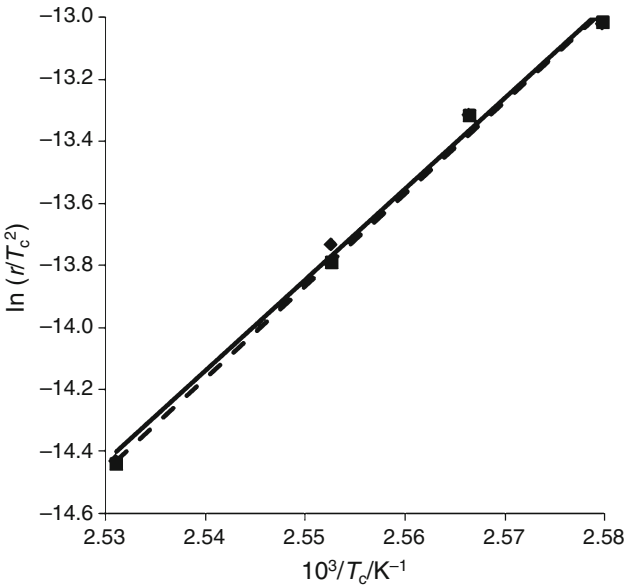

Fig. 7 Plots of $\ln(r/T_c^2)$ versus $1/T_c$ for initial (*straight line*) and oxidized iPP (*dashed line*)

$$\frac{df}{dt} = c(1-f), \tag{2}$$

where f is crystalline fraction and c is the reaction rate constant which is calculated according to Arrhenius equation:

$$c = c_0 \exp(-\frac{E_c}{kT}), \tag{3}$$

where E_c is the activation on energy of crystallization, k is the Boltzmann constant, T is the temperature, and c_0 is the frequency factor.

A plot of $\ln(r/T_c^2)$ versus $1/T_c$ is shown in Fig. 7. The slope of these straight lines gives the activation energy of crystallization E_c; the value of E_c for initial iPP is 2.513 eV and for oxidized iPP is 2.502 eV. Activation energy is the energy barrier, and the lower E_c value for oxidized iPP made the low free surface energy higher which resulted in a metal chalcogenide film interaction with oxidized iPP surface.

Conclusions

The thermo-oxidative chemical pre-treatment of iPP surface has been used to obtain interaction between hydrophobic, low surface energy polymeric surfaces and metal chalcogenides species. After chemical pre-treatment, the density of iPP changed from 0.905 to 0.910 gcm^{-3} in comparison to the value of the density of initial iPP samples. The increasing apparent density also indicated that amorphous PP with lower density and molecular mass was etched and washed from semicrystalline iPP surface. The XRD analysis has clearly confirmed that the material under study is an iPP with α (monoclinic) crystalline form. The thermo-oxidative chemical pre-treatment of iPP takes place without destruction of polymer chains and with functionalization. It led to changes in the physicochemical properties of the polymer due to chain scission and presence of carbonyl group as confirmed by FTIR and UV–Visible spectroscopic analyses. Optical studies have shown that iPP film has direct band-to-band type optical transition. The bang gap energy E_g has been found to be 5.3 ± 0.1 eV for initial iPP and 5.2 ± 0.1 eV for oxidized one. It has also been observed that the melting and crystallization temperatures reduce as carbonyl group appears. DSC results have shown that the presence of carbonyl group in oxidized iPP influences T_m and melting enthalpy; they are lower when compared to the ones of initial iPP. Melting enthalpy and crystallization energy change indicate the change in surface energy and adhesion. In summary of these results, it can be concluded that we were able to successfully modify iPP film surface compositional structure by inducing hydrophilic character via carboxylic group formation which led to the optimization of metal chalcogenide–iPP composite deposition conditions.

References

1. Alaburdaite R, Grevys S, Paluckiene E. Formation of Cu_xS layers on polypropylene sulfurized by molten sulphur. Mat Sci. 2011;17(4):399–401.
2. Krylova V, Dukstiene N. Synthesis and characterization of Ag_2S layers formed on polypropylene. J Chem. 2013;. doi:10.1155/2013/987879.
3. Krylova V, Alaburdaite R, Guobiene A. Morphological study of silver sulfide layers on the polypropylene surface. Chemija. 2013;24(1):30–8.
4. Krylova V, Milbrat A, Embrechts A, Baltrusaitis J. Ag_2S deposited on oxidized polypropylene as composite material for solar light absorption. Appl Surf Sci. 2014;301:134–41.
5. Noeske M, Degenhardt J, Strudthoff S, Lommatzsch U. Plasma jet treatment of five polymers at atmospheric pressure: surface modification and the relevance for adhesion. Int J Adhes Adhes. 2004;24:171–7.

6. Choi YH, Kima JH, Paekb KH, Jub WT, Hwanga YS. Characteristics of atmospheric pressure N_2 cold plasma torch using 60-Hz AC power and its application to polymer surface modification. Surf Coat Technol. 2005;193:319–24.
7. Rahma F, Fellahi S. Study of compatibilizers for glass fibre reinforced nylon 6/polypropylene blends. Polym Int. 2000;49:519–27.
8. Sira M, Trunec D, Stahel P, Bursikova V, Navratil Z, Bursik J. Surface modification of polyethylene and polypropylene in atmospheric pressure glow discharge. J Phys D Appl Phys. 2005;. doi:10.1088/0022-3727/38/4/015.
9. Samuels RJ. Structured Polymer Properties. New York: Wiley; 1974.
10. Maier C, Calafut T. Polypropylene: the definitive user's guide and databook. Norwich: Plastics design library; 1998.
11. Natta G, Corradini P. Structure and properties of isotactic polypropylene. Nuovo Cimento. 1960;15:40–51.
12. Zeiler T, Kellermann S, Münstedt H. Different surface treatments to improve the adhesion of polypropylene. J Adhes Sci Technol. 2000;14:619–34.
13. De Geyter N, Morent R, Leys C, Gengembre L, Payen E. Treatment of polymer films with a dielectric barrier discharge in air, helium and argon at medium pressure. Surf Coat Technol. 2007;201:7066–75.
14. Gengembre L, De Geyter N, Leys C, Morent R, Payen E, Schacht E, Van Vlierberghe S. Surface treatment of a polypropylene film with a nitrogen DBD at medium pressure. Eur Phys J Appl Phys. 2008;43(3):289–94.
15. Cui NY, Brown NMD. Modification of the surface properties of a polypropylene (PP) film using an air dielectric barrier discharge plasma. Appl Surf Sci. 2002;189:31–8.
16. Tehrani BAR, Shoushtari AM, Malek RMA, Abdous M. Effect of chemical oxidation treatment on dyeability of polypropylene. Dyes Pigm. 2004;63:95–100.
17. Leroux F, Campagne C, Perwuelz A, Gengembre L. Polypropylene film chemical and physical modifications by dielectric barrier discharge plasma treatment at atmospheric pressure. J Colloid Interface Sci. 2008;328:412–20.
18. Wang K, Wang W, Yang D, Huo Y, Wang D. Surface modification of polypropylene non-woven fabric using atmospheric nitrogen dielectric barrier discharge plasma. Appl Surf Sci. 2010;256:6859–64.
19. Du Toit FJ, Sanderson RD. Surface fluorination of polypropylene: 2 adhesion properties. J Fluorine Chem. 1999;98:115–9.
20. Steen ML, Jordan AC, Fisher ER. Hydrophilic modification of polymeric membranes by low temperature H_2O plasma treatment. J Membr Sci. 2002;204:341–57.
21. Korikov AP, Kosaraju PB, Sirkar KK. Interfacially polymerized hydrophilic microporous thin film composite membranes on porous polypropylene hollow fibers and flat films. J Membr Sci. 2006;279:588–600.
22. Pandiyaraj KN, Selvarajan V, Deshmukh RR, Gao C. Modification of surface properties of polypropylene (PP) film using DC glow discharge air plasma. Appl Surf Sci. 2009;255:3965–71.
23. Milde F, Goedicke K, Fahland M. Adhesion behavior of PVD coatings on ECR plasma and ion beam treated polymer films. Thin Solid Films. 1996;279:169–73.
24. Shreya P. Surface modification of polypropylene nonwovens to improve adhesion to elastomers. Ann Arbor: ProQuest/UMI; 2011.
25. Salkauskas M, Vaskelis A. Chimicheskaja metalizacija plastmass. Leningrad: Chimija; 1985 (in Russian).
26. Brown SD, D'Ottavio ED, Kuzmik JJ, Grunwald JJ. Method of the treating plastic substrates and process for plating thereon. Pat. USA, 3682768. 1972.
27. PDF-2 International Centre for Diffraction Data, 12 Campus Boulevard Newtown Square, PA 19073–3273 USA. http://www.icdd.com/products/pdf2.htm
28. Yang HS, Kiziltas A, Gardner DJ. Thermal analysis and crystallinity study of cellulose nanofibril-filled polypropylene composites. J Therm Anal Calorim. 2013;113(2):673–82.
29. Nishino T, Matsumoto T, Nakamae K. Surface structure of isotactic polypropylene by X-ray diffraction. Polym Eng Sci. 2000;40(2):336–43.
30. http://henke.lbl.gov/optical_constants.
31. Vychopnová J, Čermák, Obadal M, Verney V, Commereuc S. Effect of β—nucleation on crystallization of photodegraded polypropylene. J Therm Anal Calorim. 2009;95(1):215–20.
32. Rabello MS, White JR. Crystallization and melting behavior of Photodegraded Polypropylene. 1. Chemi-Crystallization. Polymer. 1997;38(26):6379–87.
33. Mishra R, Tripathy SP, Sinha D, Dwivedi KK, Ghosh S, Khathing DT, Müller M, Fink D, Chung WH. Optical and electrical properties of some electron and proton irradiated polymers. Nucl Instrum Methods Phys Res Sect B. 2000;168:59–64.
34. Pretsch E, Buehlmann P, Badertscher M. Structure determination of organic compounds: tables of spectral data. New York: Springer; 2009.
35. Tauc J, Grigorovici R, Vancu A. Optical properties and electronic structure of amorphous germanium. Phys Status Solidi. 1966; 15(2):627–67.
36. Higazy AA, Hussein A. Optical absorption studies of γ irradiated magnesium phosphate glasses. Radiat Eff Defect Solids. 1995; 133(3):225–35.
37. Stuart BH. Infrared spectroscopy: fundamentals and applications. New York: Wiley; 2002.
38. Smith BC. Infrared spectral interpretation. Boca Raton: CRC Press; 1999.
39. Klopffer W. Introduction to polymer spectroscopy. Berlin: Springer; 1984.
40. Sundell T, Fagerholm H, Crozier H. Isotacticity determination of polypropylene using FT-Raman spectroscopy. Polym J. 1996;37:3227–31.
41. Lamberti G, Brucato V. Real-time orientation and crystallinity measurements during the isotactic polypropylene film-casting process. J Polym Sci B Polym Phys. 2003;41:998–1008.
42. Treheux D, Kechaou B, Salvia M, Beaugiraud B, Juvé D, Fakhfakh Z. Mechanical and dielectric characterization of hemp fibre reinforced polypropylene (HFRPP) by dry impregnation process. Express Polym Lett. 2010;4(3):171–82.
43. Zanetti M, Camino G, Reichert P, Mülhaupt R. Thermal behavior of poly(propylene) layered silicate nanocomposites. Macromol Rapid Commun. 2001;22(3):176–80.
44. Bhattacharyya AR, Sreekumar TV, Liu T, Kumar S, Ericson LM, Hauge RH, Smalley RE. Crystallization and orientation studies in polypropylene/single wall carbon nanotube composite. Polym J. 2003;44:2373–7.
45. Zhou ZY, Cui L, Zhang Y, Zhang YX, Yin NW. Preparation and properties of POSS grafted polypropylene by reactive blending. Eur Polym J. 2008;44:3057–66.
46. Tjong SC, Meng Y. The effect of compatibilization of maleated polypropylene on a blend of polyamide-6 and liquid crystalline copolyester. Polym Int. 1997;42:209–17.
47. Avrami M. Kinetics of phase change. I. General theory. J Chem Phys. 1939;7:1103–12.
48. Avrami M. Kinetics of phase change. II. Transformation-time relations for random distribution of nuclei. J Chem Phys. 1940;8:212–24.
49. Avrami M. Granulation, phase change and microstructure kinetics of phase change. III. J Chem Phys. 1941;9:177–84.